Published online 8 August 2019

Nucleic Acids Research, 2019, Vol. 47, No. 17 ***9329–9342***
doi: 10.1093/nar/gkz668

A 212-nt long RNA structure in the Tobacco necrosis virus-D RNA genome is resistant to Xrn degradation

Chaminda D. Gunawardene, Laura R. Newburn and K. Andrew White*

Department of Biology, York University, Toronto, Ontario, M3J 1P3, Canada

Received December 04, 2018; Revised June 26, 2019; Editorial Decision July 18, 2019; Accepted July 25, 2019

ABSTRACT

Plus-strand RNA viruses can accumulate viral RNA degradation products during infections. Some of these decay intermediates are generated by the cytosolic 5′-to-3′ exoribonuclease Xrn1 (mammals and yeast) or Xrn4 (plants) and are formed when the enzyme stalls on substrate RNAs upon encountering inhibitory RNA structures. Many Xrn-generated RNAs correspond to 3′-terminal segments within the 3′-UTR of viral genomes and perform important functions during infections. Here we have investigated a 3′-terminal small viral RNA (svRNA) generated by Xrn during infections with Tobacco necrosis virus-D (family Tombusviridae). Our results indicate that (i) unlike known stalling RNA structures that are compact and modular, the TNV-D structure encompasses the entire 212 nt of the svRNA and is not functionally transposable, (ii) at least two tertiary interactions within the RNA structure are required for effective Xrn blocking and (iii) most of the svRNA generated in infections is derived from viral polymerase-generated subgenomic mRNA1. *In vitro* and *in vivo* analyses allowed for inferences on roles for the svRNA. Our findings provide a new and distinct addition to the growing list of Xrn-resistant viral RNAs and stalling structures found associated with different plant and animal RNA viruses.

INTRODUCTION

Viruses face hostile cellular environments during infections and their genomes represent key targets for cellular nucleases. The genomes of plus-strand RNA viruses are substrates both for endo- and exoribonucleases (1), and one ribonuclease that engages viral RNAs is the cytosolic enzyme Xrn1 (2). This 5′-to-3′ exoribonuclease plays a major role in eukaryotic cellular mRNA turnover by converting messages into nucleoside monophosphates (3). Access of Xrn1 to the 5′-end of mRNAs requires prior removal of the cap structure, which creates RNAs with 5′-monophosphates, the favored substrate for Xrn1 (4). This exonuclease is highly processive, however G-rich tracts and some RNA structures can impede its progress (5).

Xrn1 is a restriction factor for some plus-strand RNA viruses (6,7), however, in some cases, its activity is beneficial to infections (8,9). An example of this latter role comes from flaviviruses where, during infections, fragments that are 3′-coterminal with their plus-strand RNA genomes, termed subgenomic flavivirus RNAs (sfRNAs), are generated by Xrn1 (10). The fragments that accumulate have well defined 5′-termini and correspond to segments of the 3′-UTRs of flavivirus RNA genomes. SfRNAs have been shown to influence symptoms and to modulate viral infections in different ways, including inhibiting host Xrn1 exoribonuclease and muting the host immune response (11). The formation of sfRNAs relies on the presence of RNA sequences which form higher-order RNA structures that cause Xrn1 to stall (12–14). Notably, the atomic structures of the stalling RNAs in two flaviviruses, Murray Valley encephalitis virus and Zika virus, have been solved (15,16). These structures revealed similar complex folds which form RNA-based braces that block Xrn1 progression. Additional analyses revealed that these structures also stall other 5′-to-3′ exonucleases, suggesting a general barrier-based mechanism for hindering nuclease movement (17). This phenomenon of Xrn1 stalling and generating distinct virally-derived 5′-ends extends beyond flaviviruses. Xrn1-resistant RNAs have also been identified in other mammalian RNA viruses such as Hepatitis C virus and Bovine viral diarrhea virus (18), as well as phleboviruses and arenaviruses (19). However, the structural nature of the RNA elements responsible for these stalling events remains undetermined.

In plants, cytosolic Xrn4 is the functional equivalent of Xrn1 (20) and can either restrict (6,21) or facilitate infections (8). Similar to flaviviruses, small virally-derived 3′-terminal fragments from different plus-strand RNA plant viruses have been reported (22) and those associated with luteoviruses are among the earliest described (23–25). The origin of these luteovirus small RNAs is currently unknown, but they may be products of Xrn4 activity during plant infections. There are, however, two plant viruses,

*To whom correspondence should be addressed. Tel: +1 416 736 5243; Fax: +1 416 736 5698; Email: kawhite@yorku.ca

Beet necrotic yellow vein virus (BNYVV; genus Benyvirus, family Benyviridae) and Red clover necrotic mosaic virus (RCNMV; genus Dianthovirus, family Tombusviridae), for which generation of Xrn-resistant RNAs have been confirmed. Non-coding RNA3 (ncRNA3), is derived from genome segment RNA3 of BNYVV and is required for long-distance movement of infections in plants (26,27). NcRNA3 production *in vitro* by recombinant Xrn1 involves a 43 nt segment that forms two hairpin structures separated by a spacer sequence (28). In RCNMV, the RNA1-derived fragment that accumulates is termed SR1f, and it facilitates plant infections, possibly by regulating viral translation, replication, or packaging (29). For RCNMV, a 43 nt long sequence is also needed for Xrn1 stalling, but its sequence is distinct from that in BNYVV (30). The crystal structure of the RCNMV stall signal inferred an RNA fold that could act as a brace against Xrn4, however, its conformation is distinct from those found in flaviviruses (30).

In addition to RCNMV, small 3′-terminal, genome-derived, RNAs have been reported for other members of the family Tombusviridae, but they have not been characterized (31–34). This group includes Tobacco necrosis virus-D in the genus Betanecrovirus, which has a ∼3.8 kb plus-strand RNA genome that is packaged into an icosahedral particle (35). The genome is neither 5′-capped nor 3′-poly(A) tailed and encodes five open reading frames (ORFs) (Figure 1A). Upon infection, the accessory replication protein (p22) and its readthrough product (p88), the RNA-dependent RNA polymerase, are translated directly from the genome (36,37). Translation is mediated by an RNA structure in the 3′-untranslated region (3′-UTR) termed the 3′ cap-independent translational enhancer (3′-CITE), which functions by binding to eukaryotic initiation factor 4G (eIF4G) (38,39). The 3′-CITE also supports translation of two subgenomic (sg) mRNAs that are transcribed during infections (32). Two small proteins that mediate virus movement within the plant, p7a and p7b, are expressed from the larger sg mRNA1, while the viral capsid protein (CP) is translated from sg mRNA2 (40) (Figure 1A).

Here, a 3′-terminal small viral RNA (svRNA) associated with TNV-D infections was investigated. The results indicate that it is generated by Xrn4 digestion and that a complex RNA structure is involved in the stalling event leading to its formation. Possible functions of this svRNA are investigated and discussed.

MATERIALS AND METHODS

TNV-D constructs

The full-length infectious TNV-D clone (GenBank D00942.1) has been reported previously (35), and all mutants were derived from this construct. The TNV-D sg mRNA1 (initiating at genome coordinate 2216) and sg mRNA2 (coordinate 2557) clones were generated as described previously (40). Standard overlapping PCR-based mutagenesis was used to introduce mutations into the genomic or subgenomic RNA clones of TNV-D. All clones were sequenced to ensure the presence of only the intended modifications.

In vitro transcription and viral RNAs

All RNA transcripts were generated by *in vitro* transcription of either SmaI-linearized clones or 3′-ends that were delineated by PCR-products, as described previously using a T7-FlashScribe transcription kit (41). Capped luciferase and wasabi mRNAs were transcribed from linearized expression vector using an AmpliCap-Max T7 Transcription Kit. Transcript integrity was verified by agarose gel electrophoresis prior to use. Transcript 50-svRNA, included the fifty contiguous viral nucleotides 5′-proximal to the primary Xrn termination site and was used for in-line probing and Xrn1 inhibition assays.

Protoplast infections and northern blot analysis

Protoplasts were isolated from 6- to 7-day-old cucumber cotyledons as described previously (42). Following isolation, 3×10^5 protoplasts were transfected with 5 μg of genomic TNV-D transcripts, mediated by PEG-$CaCl_2$. Transfected protoplasts were incubated under constant light for 22 h at 22°C. Total nucleic acids were phenol extracted and ethanol precipitated, after which one-sixth of the preparation was separated in 2% agarose gels and transferred to nylon membrane. Northern blot analysis was carried out using two internally-labeled ^{32}P-labeled DNA oligonucleotide probes that were complementary to two different regions of the 3′-UTR of TNV-D that did not overlap with regions containing nucleotide substitutions in mutants: GACTGGGTTCCTAGAGAGATCTCTAGGTAAATAAAGAGGGGAC-3′(−), complementary to the 3′-terminal 39 nts of the viral genome (coordinates 3725–3763, underlined), and GTGATACGACGGCCCACCACCACAGTGAGCCCGTTAAACCTGTTTCCCAGGATCC-3′(−) complementary to the apical sequence of the BTE structure (coordinates 3592–3646). Both probes were used for all northern blot analyses, except for the BTE truncation mutants, where only the 3′-terminal probe was used (due to overlap between the BTE deletions and the BTE-targeted probe) (36). Probes were generated using Klenow fragment (NEB Cat# M0210L) using primer/template pairs. 3′-Terminal probe: template (+)5′-GTCCCCTCTTTATTTACCTAGAGATCTCTCTAGGAACCCAGTC and primer (−)5′-GACTGGGT. BTE-targeted probe: template: (+)5′-GGATCCTGGGAAACAGGTTTAACGGGCTCACTGTGGTGGTGGGCCGTCGTATCAC and primer (−)5′-GTGATACG). Probes were synthesized using 5 U of Klenow fragment in the presence of [α-^{32}P]-dATP and unlabeled CTP, GTP and TTP for 1 h at 25°C. Labeling reactions were stopped using 20 mM EDTA and purified via G50 sephadex columns. All protoplast infection experiments were repeated three times.

In vitro Xrn1 digestion assay

Purified Xrn1 from *Saccharomyces cerevisiae* was obtained from New England Biolabs (NEB) (Cat# M0338L). Buffer conditions for reactions were followed as described previously (14). Briefly, 2 μg of wild-type (wt) or mutant sg mRNA1 were incubated in 1× EC3 buffer (100 mM NaCl, 10 mM $MgCl_2$, 50 mM Tris, pH 7.9, 1 mM DTT) with 0.5

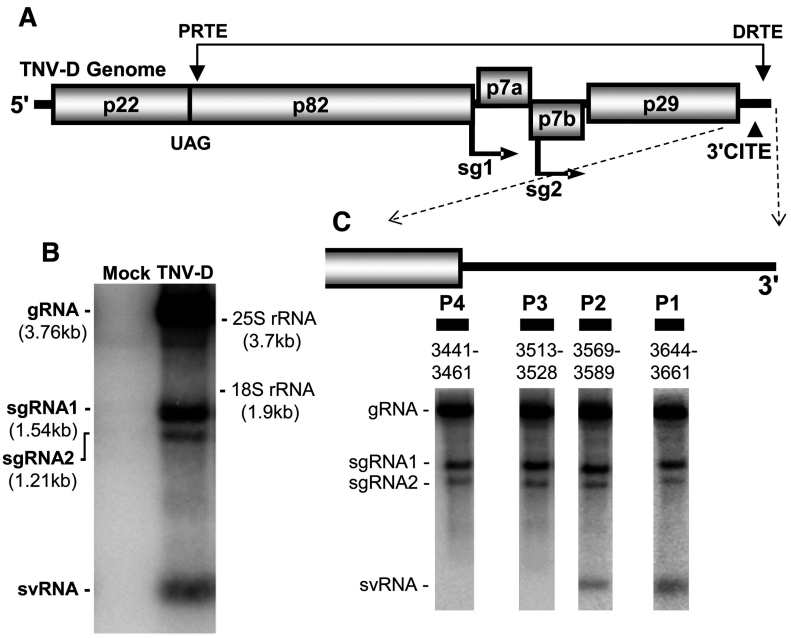

Figure 1. TNV-D genome and identification of svRNA. (**A**) Schematic representation of the TNV-D genome with encoded proteins shown as rectangles. The initiation sites of the two subgenomic (sg) mRNAs are marked below by arrows. Positions of the 3′-cap-independent translation enhancer (3′-CITE) and the complementary proximal and distal readthrough elements (PRTE and DRTE, respectively) are also shown. (**B**) Northern blot of TNV-D infection in plant protoplasts. Total RNA was separated in 2% agarose gels, transferred to nylon membrane and hybridized with ^{32}P-labelled oligonucleotides complementary to different 3′-regions of the TNV-D genome. The positions of genomic (g), subgenomic (sg) and small viral (sv) RNAs in the blots are identified to the left. The position and sizes of relevant RNAs are also shown. (**C**) Northern blot delineating the approximate 5′-end of the svRNA. The relative genomic positions of the probes (P1 to P4) are shown along with their corresponding genome coordinates.

U Xrn1 and 4 U RppH (derived from *Escherichia coli*, obtained from NEB, Cat# M0356S) in the presence of 20 U RNase inhibitor in a volume of 23 μl at 37°C for 30 min. RNA was ethanol precipitated with 20 mg glycogen and 0.2 M ammonium acetate, and dissolved in RNase-free water. Two-fifths of the RNAs recovered was separated in 2% agarose gels and transferred to nylon membrane for northern blot analysis. The signal strengths from bands were quantified using QuantityOne software. All assays were repeated three times. The level of resistant svRNA was calculated as a ratio: i.e. the level of resistant RNA divided by the level of untreated precursor, which was set as 100%. Representative northern blots used for quantification of svRNAs in Figures 3D and 4A are provided in Supplemental Material.

5′-RACE

RNAs extracted from TNV-infected protoplasts or generated by digestion with Xrn1 *in vitro* were separated in 2% agarose gels. Bands corresponding to the svRNA were excised as gel slices and the extracted RNA was ligated to an oligonucleotide adaptor sequence containing an SbfI site (bold): 5′-GATCTGCAGCTTGAG**CCTGCAGG**GTGCTGCGCAGAGTTCTACAGTCCGAC using T4 RNA ligase (NEB). RT-PCR was carried out using a reverse primer complementary to the genome 3′-terminus (underlined) and containing a SalI site (bold), 5′-GCAGCA**CGTCGAC**GGGTTCCTAGAGAGATCTCTAGG, and nested primer 5′-GCAGCTTGAGCCTGCAGGGTGC. PCR products were double-digested with SbfI and SalI and ligated into a pUC19 vector, cloned into *E. coli*, and individual clones were sequenced.

In-line probing

Wt and mutant 50-svRNAs were transcribed *in vitro*. Following 5′-end-labeling using [γ-^{32}P]-ATP, RNAs were incubated for ∼40 h at 25°C and then separated in 10% sequencing gels (43). The signal strengths from bands in each lane were quantified using QuantityOne software and plotted together.

In vitro translation competition assay

Uncapped wt TNV-D genomic (0.1 pmol), sg mRNA (0.2 pmol), capped reporter luciferase mRNA or wasabi mRNA (0.2 pmol) (Luciferase-pcDNA3, pTcI-Wasabi, obtained from Addgene) were incubated with increasing molar excesses (1:1 ratio up to 1:64) of uncapped wt svRNA or a size-matched uncapped RNA control, derived from pUC19, 5′-CUGGCGAAAGGGGGAUGUGCUGCAAGGCGA UUAAGUUGGGUAACGCCAGGGUUUUCCCAG UCACGACGUUGUAAAACGACGGCCAGUGAA UUCGAGCUCGGUACCCGGGGAUCCUCUAGA GUCGACCUGCAGGCAUGCAAGCUUGGCGUAAU CAUGGUCAUAGCUGUUUCCUGUGUGAAAUU GUUAUCCGCUCACAAUUCCACACAACAUAC, in a wheat germ extract translation system (Promega) (36). Reactions of 20 μl included 10 μl wheat germ extract and were incubated at 25°C for 2 h.

In vitro Xrn1 inhibition assay

A Xrn1-sensitive, 50 nt long, non-viral reporter RNA (Rep) 5′-GGAACAGACAGACAUACAGACGCAGA CACACACACACACACACACACACA, was used to assess the protective effect of (i) wt 50-svRNA, (ii) a mutant 50-svRNA (50-S6C) or, (iii) a size-matched, non-viral RNA sequence (NS) derived from pUC19 (i.e. the size-matched sequence provided in previous section plus the following 50 nt sequence added to its 5′-end: GAGCCGGAAGCAUAAAGUGUAAAGCCUGGG GUGCCUAAUGAGUGAGCUAA). Rep and competitor RNAs were *in vitro* transcribed with a 10-fold molar excess of GMP over GTP to generate transcripts with 5′-monophosphates, thereby obviating the need to add RppH, which could potentially be rate limiting for Xrn1 activity. Mixtures of the Rep RNA (3 ng) and each of the competitor RNAs [(i), (ii) or (iii); 1 μg each] were incubated for 1 min in the absence or presence of 1 U Xrn1 at 37°C. Upon completion of the reactions, RNA was phenol extracted, ethanol precipitated, separated in a 2% agarose gel, transferred to nylon membrane, and probed for Rep RNA.

Whole plant infections and particle isolation

Three week old *Nicotiana benthamiana* plants were rub-inoculated with transcripts of either wt or mutant genomic TNV-D RNAs as described previously (44). Plants were incubated at 23°C with a 14 h/10 h day/night cycle until developing visible symptoms (∼6 days). Three plants were inoculated for each viral construct per experiment, and each experiment was repeated three times. RNA was extracted from symptomatic inoculated or upper leaves and analyzed by northern blotting. For virion preparations, plants were inoculated and incubated as described above. Virus particles were prepared from systemically-infected leaf tissue via PEG precipitation (45) and RNAs extracted from virus particles were analyzed by northern blotting as described earlier.

RESULTS

TNV-D infections contain a 3′-terminal small viral RNA

Infections of cucumber protoplasts with wt TNV-D were examined for the accumulation of viral RNAs using a probe complementary to the very 3′-terminus of the viral genome. Northern blot analysis revealed that, in addition to the expected genome and two sg mRNAs, a small viral RNA (svRNA) was detected consistently (Figure 1B). To assess how much sequence from the 3′-terminus was present in the svRNA, additional oligonucleotide probes were utilized that spanned more upstream regions of the 3′-UTR and extended into the adjacent p29 capsid-coding region. This analysis indicated that the 5′-end of the svRNA mapped between oligos-3 and -2, with the intervening sequence corresponding to genome coordinates 3528–3569 (Figure 1C). Based on these results, the size of the svRNA was estimated to be between 195 and 235 nt in length, a size consistent with its high mobility in agarose gels.

The svRNA is analogous to the products of Xrn1-digested TNV-D RNAs

The presence of Xrn1-generated 3′-terminal fragments in other plus-strand RNA virus infections prompted us to investigate the same possibility for the TNV-D svRNA. Accordingly, *in vitro* transcripts of TNV-D genomic and sg mRNAs were individually subjected to recombinant yeast Xrn1 in the presence of pyrophosphohydrolase RppH, which converts 5′-triphosphates in the transcripts to 5′-monophosphates (14). In this assay, all three viral species that were subjected to Xrn1 and RppH yielded an RNA product that comigrated to the same position as the svRNA generated in protoplast infections (Figure 2A, middle and right sections). When the 5′-termini of Xrn1-generated RNAs and *in vivo*-generated svRNA were cloned and sequenced by 5′-RACE (Figure 2B), the most frequent positions mapped to two adjacent nucleotides located just 5′-proximal to the basal stem structure of the 3′-CITE; corresponding to genomic coordinates 3552 and 3553 (Figure 2C, green asterisks). 5′-termini at these positions would yield svRNAs of lengths 211 and 212 nts, which are within with the size range estimate of 195–235 nt determined by oligonucleotide probing (Figure 1C). This equivalence in gel mobility and 5′-termini location between *in vitro*-generated small RNAs and *in vivo*-generated svRNAs is consistent with the latter being produced by plant Xrn4, the counterpart to yeast Xrn1 (28). These results also indicate that no *trans*-acting cellular or viral proteins are required for this process to occur.

svRNAs are derived primarily from sg mRNA1

In flaviviruses, which do not produce traditional protein-coding sg mRNAs, the lone source of Xrn-resistant RNAs is the viral genome. However, for TNV-D, which synthesizes two sg mRNAs during infections, either or both messages could contribute to production of svRNAs in infections. To examine this possibility, genomic mutants were assessed that were deficient in transcription of either sg mRNA1 or sg mRNA2, due to point mutations in their initiating nucleotides (Figure 2D). Inhibition of sg mRNA1 transcription resulted in a large decrease in svRNA accumulation in protoplasts, while inactivation of sg mRNA2 had nominal effects. Accordingly, most of the svRNA that accumulates during infections is derived from sg mRNA1.

Structural and functional features of the svRNA

The 3′-region of the TNV-D genome has been well characterized, both structurally and functionally. The major Xrn1-resistant fragment corresponds to a 212 nt long 3′-terminal segment that contains several functional subregions (Figure 2C). At the 5′-end is the 3′-CITE, which is composed of an extended stem structure topped by two stem-loops (SLs) (38,39,46). Just downstream from the 3′-CITE are

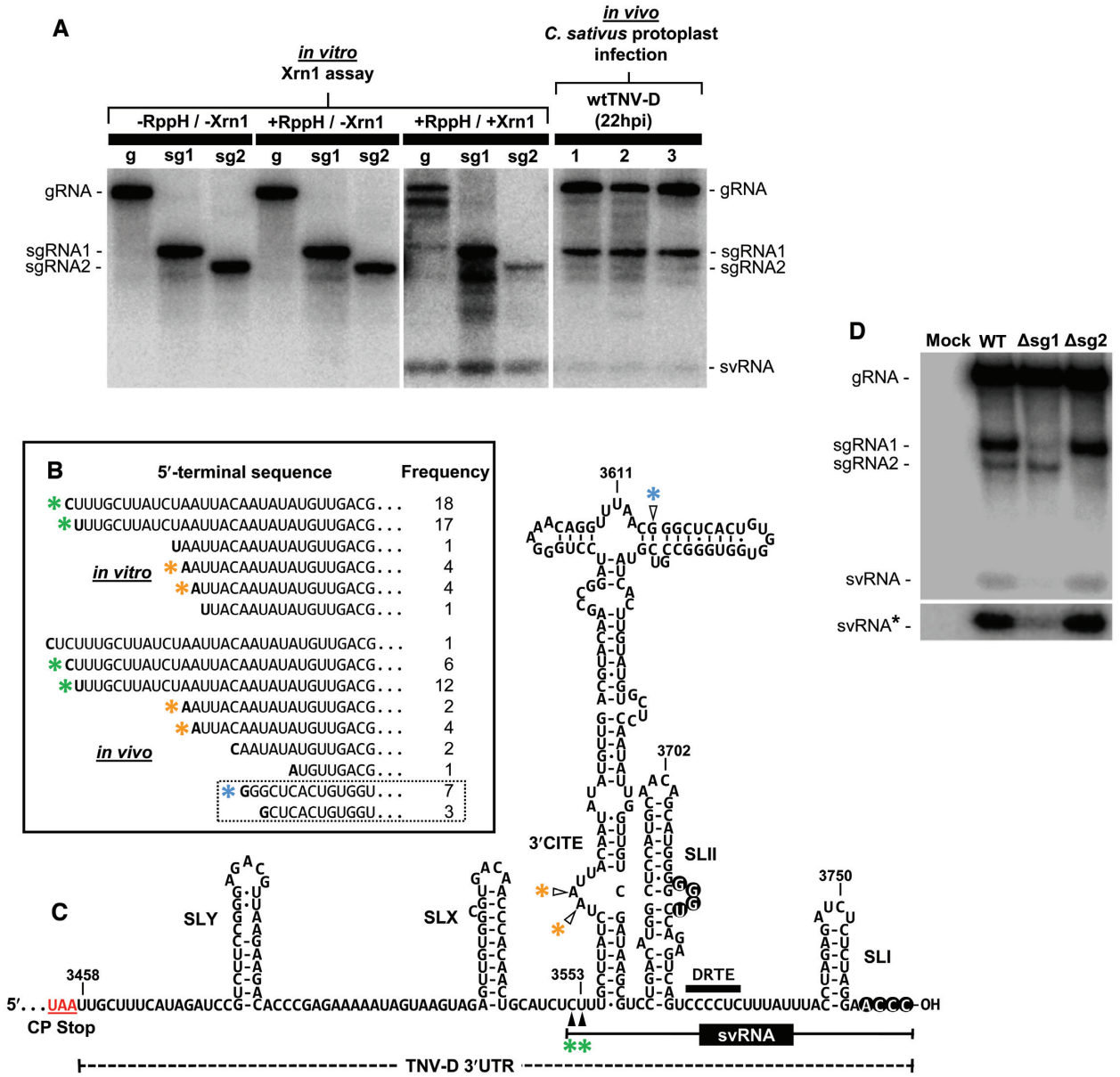

Figure 2. Comparison of *in vitro* and *in vivo*-generated svRNAs. (**A**) Northern blot comparing *in vitro*-derived svRNA produced by Xrn1 and svRNAs produced in protoplast infections. Treatment of viral RNA transcripts with (+) or without (−) RppH and Xrn1 are indicated above the lanes. All sections shown are from the same gel. (**B**) 5′-RACE analysis of svRNAs produced by Xrn1 (*in vitro*) and svRNAs produced in protoplast infections (*in vivo*). 5′-terminal sequences are shown with their corresponding frequency of occurrence. The dotted box encloses minor stall sites with 5′-ends that originate further downstream than the other sequences shown and are not aligned with those sequences above. (**C**) Secondary structure of the 3′-UTR of TNV-D. Substructures, including SLI, SLII and the 3′-CITE are indicated. Colour-coded asterisks correspond to 5′ nucleotide positions from sequence termini shown in (B). The major svRNA species (i.e. 211–212) is indicated below the structure. Complementary nucleotides in SLII and the 3′-terminus that functionally base pair are circled. (**D**) Northern blot analysis of protoplast infections of TNV-D genomes with inactivated sg mRNA1 (Δsg1) or sg mRNA2 (Δsg1) promoters. The lower panel labelled svRNA* is a longer exposure of the svRNA-containing portion of the blot above.

two hairpins, SLII and SLI. Both stem loops are critical for genome replication, as is a base pairing interaction between the 3′-terminal four nucleotides and an internal bulge in SLII (Figure 2C, circled nucleotides) (37). These two hairpins flank a 6 nt long sequence, the distal readthrough element (DRTE), which can base pair with a complementary proximal RTE (PRTE) that is present in an RNA structure 3′-adjacent to the p22 stop codon. This RNA-RNA interaction mediates translational readthrough resulting in production of p82 (Figure 1A) (36). The svRNA thus contains regulatory elements involved in translation initiation, translational readthrough, and genome replication.

Terminal regions of svRNA contain determinants of Xrn1 resistance

To examine structural features important for svRNA production we utilized transcripts of sg mRNA1 as an *in vitro* substrate for Xrn1, which, on average, generated 4.3%

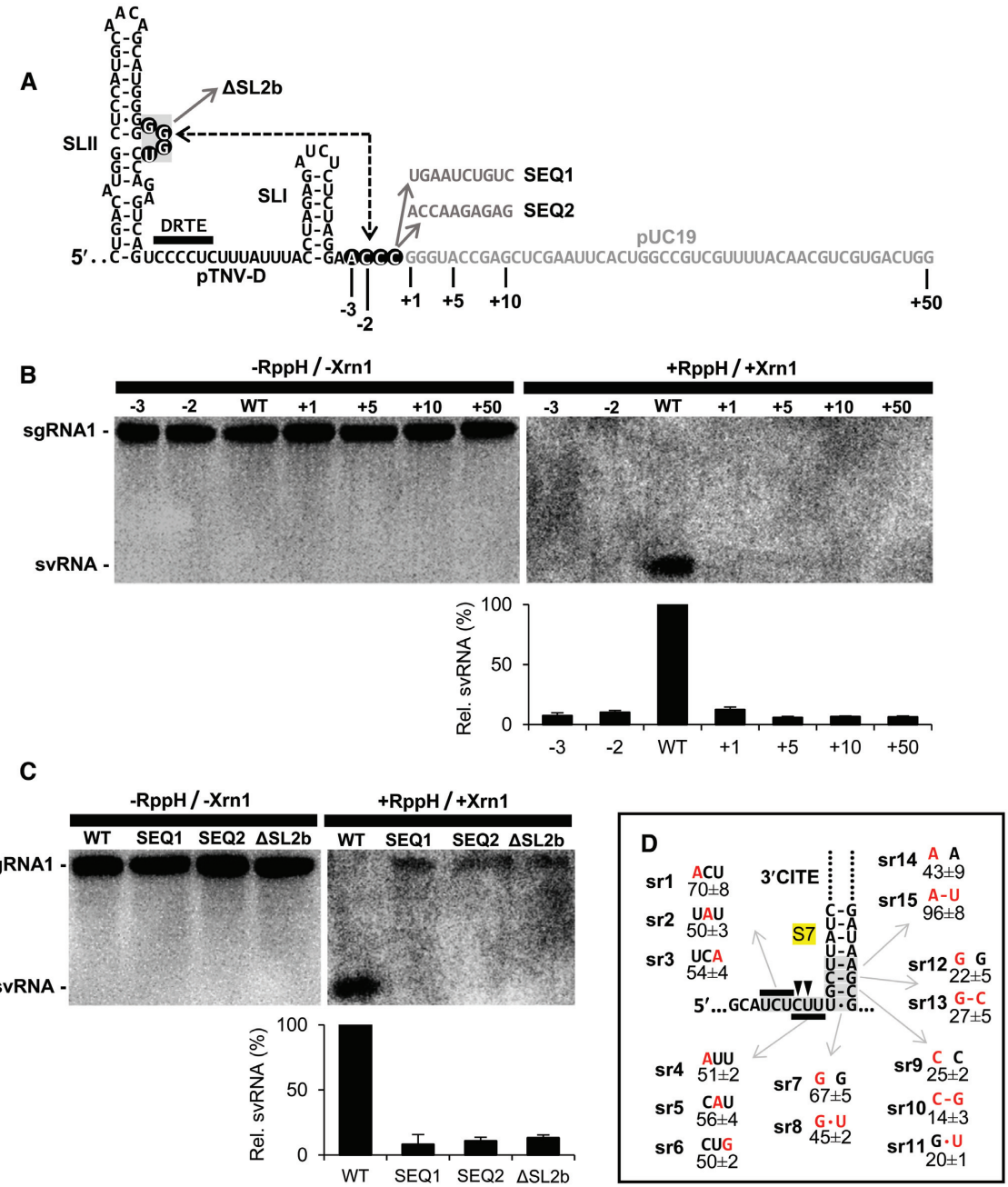

Figure 3. Mutational analysis of the 5′- and 3′-terminal regions of the svRNA in sg mRNA1. (**A**) Nucleotides were either added (from pUC19) or deleted from the 3′-end of TNV-D sg mRNA1. The SLII/3′-end interaction important for genome replication is indicated with dotted arrows. Modifications and the associated mutant names are shown. (**B** and **C**) *In vitro* Xrn1 assay of sg mRNA1 mutants depicted in (A). The substrate and product RNA species are labelled to the left, and a bar graphs below the blots quantify corresponding svRNA levels from three independent experiments, ±SE. (**D**) Mutational analysis of the 5′-terminal region of svRNA in sg mRNA1. Substitutions in each mutant are shown in red along with relative levels of accumulation of svRNAs (from three independent experiments, ±SE). Stem 7 (S7) of the 3′-CITE is highlighted in yellow. Black arrowheads indicate the primary Xrn1 stall sites.

svRNA (±0.7%, $n = 10$) from a reactant pool of sg mRNA1 set as 100%. An interesting feature of previously reported Xrn-blocking viral RNA structures is their modularity, whereby they are still functional when introduced into new sequence contexts (14,29). To assess this aspect of function, the normal 3′-terminus of sg mRNA1 was extended by one, five, ten, or fifty nucleotides of adjacent plasmid sequence (Figure 3A). Two other 10 nt 3′-terminal extensions of differing nucleotide order and composition, mutants SEQ1 and SEQ2, were also assessed, in addition to another mutant, ΔSL2b, containing a deletion of the bulge in SLII (Figure 3A). Transcripts were also produced that lacked two or three nucleotides from the 3′-end. When these viral RNAs were assayed for svRNA production *in vitro*, all modifications resulted in greatly decreased levels of svRNA (Figure 3B and C). Accordingly, small and large indels at

the 3′-terminus of the substrate RNA have major effects on its ability to stall Xrn1; as did deletion of the bulge in SLII, which is the base pairing partner sequence for the 3′-terminus (Figure 3A).

The 5′-terminus of the primary svRNA corresponds to the 5′-border of the 3′-CITE. This position would also be the location of the Xrn1 active site when the enzyme is stalled, and nearby nucleotide residues and/or RNA structures are predicted to affect this event. The substitution of single nucleotides positioned before, within, or after the major stall sites had varying effects (Figure 3D). Those changes corresponding to the region in front of (mutants sr1 to sr3) or at (sr4 and sr5) the stall sites reduced svRNA production to ∼50–70% that of wt levels, while the majority of those mapping within the closing stem of the 3′-CITE (sr7 to sr15) had more substantial negative effects (Figure 3D). For example, two of the four single substitutions in the left half of this closing stem (i.e. sr9 and sr12) caused drops in accumulation to 22% and 25% that of wt, with no or low recovery in corresponding compensatory mutations (Figure 3D). When combined with the results from analyses of the 3′-terminus, the data indicate that both ends of the svRNA contribute notably to Xrn1 stalling.

Internal regions of the svRNA confer Xrn1 resistance

The largest structural component within the svRNA is the 3′-CITE. Based on the results presented in the previous section, the closing stem of this structure, S7 (Figure 4A), is important for Xrn1 stalling. To assess the possible involvement of other parts of the 3′-CITE, truncations were designed in an sg mRNA1 substrate that progressively removed upper sections of the structure and replaced them with a terminal ultra-stable cUUCGg tetraloop (47). Deletion of upper portions in mutants ΔTop and Midi resulted in reduced levels of svRNA (∼57% and 38% of wt) (Figure 4A, green). Removal of additional structure in Mini markedly reduced svRNA accumulation (∼3% of wt), implicating the midsection of the 3′-CITE as particularly important for stalling.

Next, the structural requirements within the mid and lower regions of the 3′-CITE were investigated in more detail. Substitutions in stem 4 in mutant series S4 resulted in moderate effects that supported a role for base pairing, while those in stem 5 (series S5) had similar effects without implicating base pairing as being important (Figure 4A). Compensatory mutation sets in lower stems 6 and 7 in mutant series S6 and S7 yielded major defects in svRNA levels (i.e. down to ∼10%) and restoration of base-pairing did not recover function. Changes to the asymmetrical loop between stems 6 and 7 in series IL6, and mismatches between stems 5 and 6 in series IL5, also notably inhibited activity (∼17–23% and ∼21–57%, respectively), while perturbation of another helical interruption further up the structure in mutant ΔGCUC was well tolerated (99%) (Figure 4A). These results agree with those from internal truncations of the 3′-CITE and Figure 3C, with all findings implicating the lower region of the 3′-CITE as most important for Xrn1 stalling activity.

SLII was also investigated for possible involvement with Xrn1 stalling activities. Compensatory mutational analysis indicated that base pairing in the lower (m106, m107 and m108), middle (m135, m136 and m137), and near-upper regions (m132, m133, and m134; and m129, m130 and m131) of SLII contributed to its function, albeit to differing degrees (Figure 4A). Restoration of canonical complementarity in the base pair closing the terminal loop, did not improve svRNA production (mutants m126, m127 and m128). Also notable, was that any of eight different changes made in the terminal loop of SLII caused major decreases in svRNA production (∼14–29% of wt) (Figure 4A). Collectively, the results from examining the internal sections of the svRNA implicate SLII and the mid/lower part of the 3′-CITE as highly important elements for stalling Xrn1.

Regions within the svRNA that were required for efficient svRNA production, and which appeared to be highly dependent on sequence specificity, included the lower region of the 3′-CITE (i.e. stems 6 and 7 and their intervening internal loop) and the upper region of SLII (i.e. its terminal loop region). Accordingly, we examined the structural consequences of certain modifications in these regions by in-line probing, a solution structure analysis method that identifies flexible residues in an RNA by their propensity to undergo spontaneous cleavage (43). The viral RNAs analyzed were based on 50-svRNA, which, in addition to the svRNA sequence, contains fifty contiguous viral nucleotides 5′-proximal to the primary Xrn termination site. Like sg mRNA1, this 50-svRNA is a substrate for Xrn1, but, because its 5′-end is much closer to the stall site, analysis of reactivity in this region was more feasible. For mutant m20, which contained an AACA to GAAA substitution of the SLII terminal loop sequence and exhibited ∼29% activity, spontaneous RNA cleavage was notably increased in the region of the modified loop (Figure 4B, top trace, red asterisk) when compared to the wt control (Figure 4B, bottom trace). This suggests that these terminal loop residues are normally inflexible in the wt structure and thus may interact with other residues. Interestingly, the same loop modification also led to a small, but reproducible, increase in reactivity in the 5′-half of S6 and the adjacent asymmetrical internal loop region of the 3′-CITE (Figure 4B, top trace, green asterisk), when compared to the wt control. This result implies a structural connection between the SLII terminal loop and the lower half of the extended helix of the 3′-CITE. This notion was further supported by the analyses of mutants S6C (∼14% activity) and IL6C (∼17% activity), containing perturbations in the S6 and adjacent asymmetrical internal loop region of the 3′-CITE (Figure 4B, second and third traces, red asterisks), which induced prominent cleavages in the SLII loop region (Figure 4B, second and third traces, green asterisks). In contrast, mutant sr10 (∼14% activity) at the base of the 3′-CITE did not cause notable cleavage in the SLII loop or elsewhere. The coupled structural effects observed for mutants m20, S6C and IL6C suggest that the loop of SLII needs to interact with the lower region of the 3′-CITE to form an effective blocking structure.

Comparison of Xrn1 sensitivity *in vitro* with svRNA accumulation in virus infections

To assess how closely *in vitro* results reflected those from *in vivo* studies, several mutations that were assayed for Xrn1

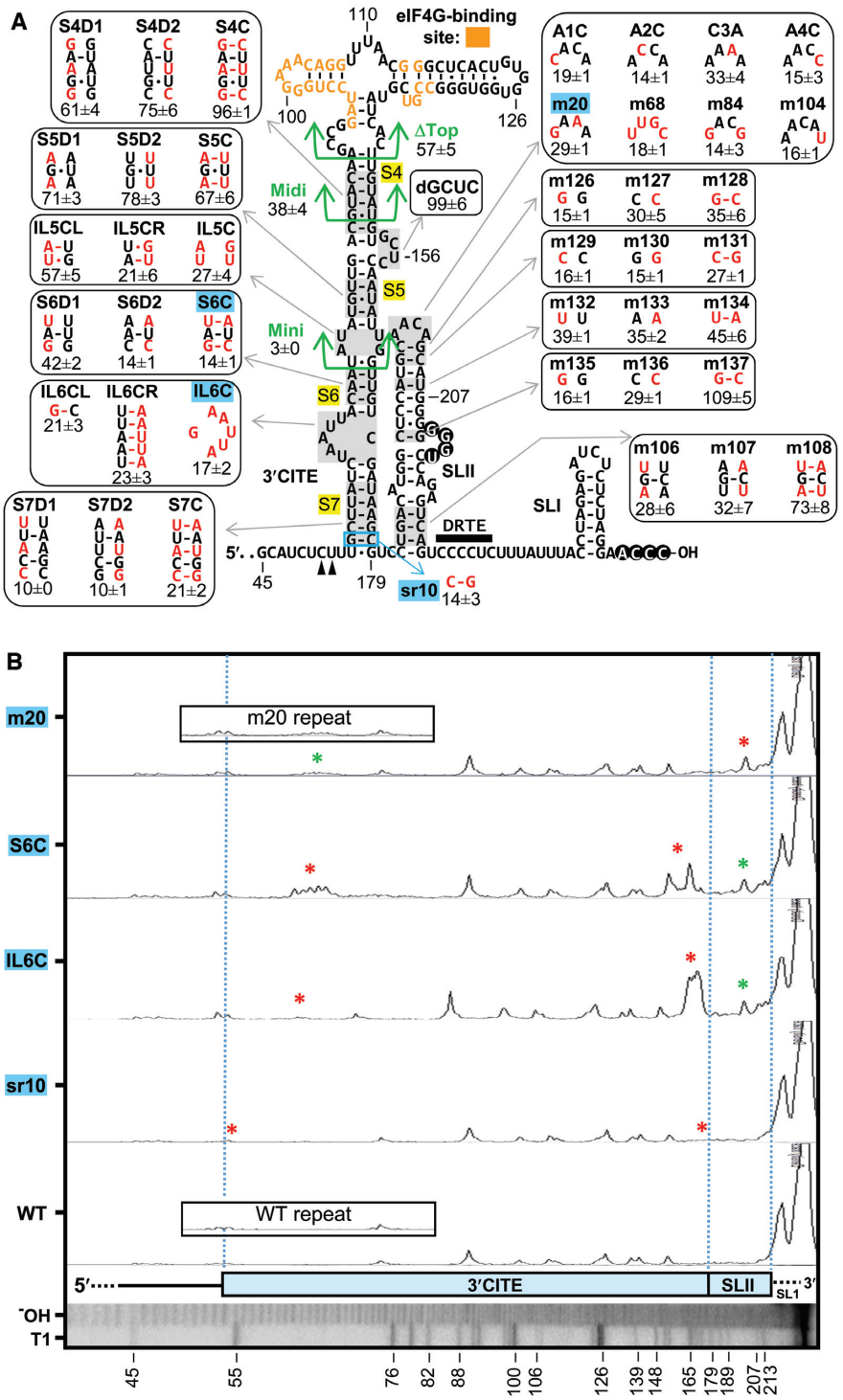

Figure 4. Mutational analysis of internal regions of the svRNA in sg mRNA1 and RNA structural analysis of selected 50-svRNA mutants defective at generating svRNAs. (**A**) Summary of *in vitro* Xrn1 assays of sg mRNA1 mutants containing substitutions or deletions in the 3′-CITE and SLII. Nucleotide substitutions in mutants are shown in red and deleted regions are outlined in green. The nucleotides in the 3′-CITE shown previously to interact with the translation factor eIF4G are shown in orange (39). Stems in the 3′-CITE are highlighted in yellow and numbered (S4 through S7). Mutants assessed by in-line probing in (B) are highlighted in blue. The primary stall sites are marked with black arrowheads below the structure. Results are from three independent experiments, ±SE. (**B**) In-line probing of svRNA-deficient mutants. The mutants assessed are shown in (A) and are highlighted in blue. *In vitro* transcripts of wt and mutant 50-svRNAs were used in the analysis and RNA reactivity for each sample was graphed. Alkaline hydrolysis (⁻OH) and T1 nuclease-treated (T1) lanes are shown along with numbering of corresponding G residues. Also shown below the profiles is a schematic depicting relevant substructures in the RNA and blue dotted lines indicate border locations of the 3′-CITE and SLII. Red asterisks indicate the positions of the modifications introduced and green asterisks indicate second-site changes in reactivity observed elsewhere in the structure. Independent repeats are shown in the insets for m20 and wt. Note that peaks in the 3′-CITE region of IL6C are shifted to the left due to the transposition of different numbers of residues in this mutant.

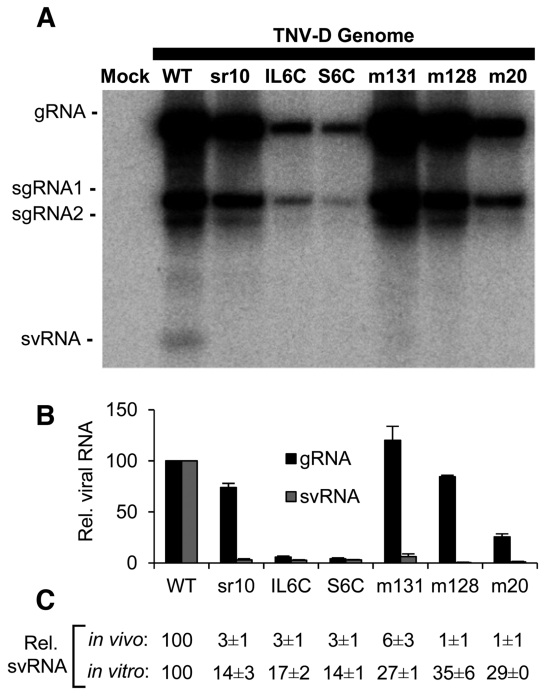

Figure 5. Replication of selected svRNA-deficient viral genomic mutants in protoplasts. (**A**) Northern blot analysis of selected mutants. Mutants are listed above the lanes and viral RNA species are labelled on the left. (**B**) Graphical representation of relative genome replication and svRNA production in (A). Black bars indicate genome replication and grey bars represent svRNA production. (**C**) Comparison of *in vivo* and *in vitro* svRNA production. *In vivo* values are derived from quantitative analysis shown in (B) and *in vitro* values were taken from Figure 4. Results are from three independent experiments, ±SE.

sensitivity (Figure 4A) were introduced into the full-length infectious clone of TNV-D and tested in protoplast infections (Figure 5A). Genome accumulation was most severely affected for IL6C, S6C and m20, containing changes to the asymmetrical internal loop, S6, or the terminal loop of SLII, respectively (Figure 5B). Thus, some changes that inhibit svRNA production *in vitro* also have major negative effects on essential viral processes. In contrast, near wt levels of genome were observed for sr10, m131 and m128 (Figure 5B). However, for these cases, the relative levels of svRNA observed *in vivo* were lower than corresponding *in vitro* levels (Figure 5C). Such differences may be a consequence of the more complex cellular environment during infections. Nonetheless, collectively, these results show that mutants exhibiting notable defects in svRNA production in *in vitro* assays also show diminished ability to generate svRNAs during infections (Figure 5C).

Functional analyses of svRNA

To gain insights into the possible function(s) of svRNA during infections, we assessed the ability of a precursor svRNA to inhibit viral RNA translation *in vitro*. We reasoned that the presence of the 3′-CITE within the svRNA could act as a sponge for eIF4F, and thus sequester this factor away from authentic viral RNAs, as was shown previously using only the TNV-D 3′-CITE as competitor (39). To test this idea, increasing amounts of svRNA or a size-matched non-specific (NS) RNA were added to *in vitro* translation reactions containing a fixed amount of either genomic or sg mRNA (Figure 6A–C). In all cases, increases in translation were observed with the NS competitor, which is likely due to it interacting non-specifically with inhibitory factors in the translation extract. For the viral RNAs, svRNA addition resulted in dose-dependent inhibition of viral RNA translation to ∼50%, at the highest level of competitor (Figure 6A–C). In contrast, similar competition assays performed with two different capped reporter mRNAs and the svRNA effectively prevented translation at the highest concentration of svRNA tested (Figure 6D and E). Thus, the svRNA can compete against both uncapped viral RNAs and capped mRNA, but is notably more effective at suppressing translation of the latter.

A second possible function of the svRNA could be to sequester Xrn1, if the enzyme stays paused at stall sites for extended periods of time. For this analysis, an Xrn1-sensitive non-viral RNA was used as a reporter (Rep). The reaction also contained either, no added RNA (M), 50-svRNA, a 50-svRNA mutant containing the S6C modification (50-S6C), or a size-matched NS RNA (Figure 7A). The Rep RNA was efficiently digested by Xrn1 in the absence of a competitor RNA. However, although all added competitor RNAs conferred a level of resistance to Xrn1, the wt viral-based 50-svRNA substrate provided the least protection when compared to the two controls. Assays were also conducted with different concentrations of Rep, competitor RNAs, and Xrn1, as well as at multiple time points, however similar results to those presented were observed in all cases (data not shown). Consequently, the findings indicate that under the conditions tested, the presence of the Xrn1 pausing sequence does not provide added protection from Xrn1 digestion to other RNAs.

A third possible function for the svRNA could be related to the assembly of viral particles. In this case, the svRNA could be included as part of the nucleic acid content of virions. To assess this possibility, we inoculated *N. benthamiana* plants with transcripts of wt TNV-D genome and isolated virus particles from infected leaves. The nucleic acid content of the isolated virus particles was subsequently assessed by northern blotting. This analysis indicated that small amounts of the two viral sg mRNAs, as well as svRNA, are packaged in TNV-D virus particles (Figure 7B).

Lastly, we wanted to determine if the absence of svRNA in whole plant infections would result in a noticeably altered phenotype. Mutant sr10 was selected for this analysis because (i) it had near wt levels of infection in protoplasts and trace levels of svRNA *in vitro* and *in vivo* (Figure 4), (ii) its modification was distal to the upper functionally-relevant region of the 3′-CITE needed for viral protein translation (38), (iii) the mutation was away from the terminal loop of SLII, which is critical for efficient translational readthrough of p82 (37) and (iv) the substitutions in it did not induce any noticeable structural changes to other regions in the svRNA (Figure 4B). *N. benthamiana* plants were rub-inoculated with transcripts of wt or sr10 mutant TNV-D genomes. At 6 days post infection, leaves inoculated with wt transcripts showed leaf curling, yellowing, and necrosis (Figure 7C).

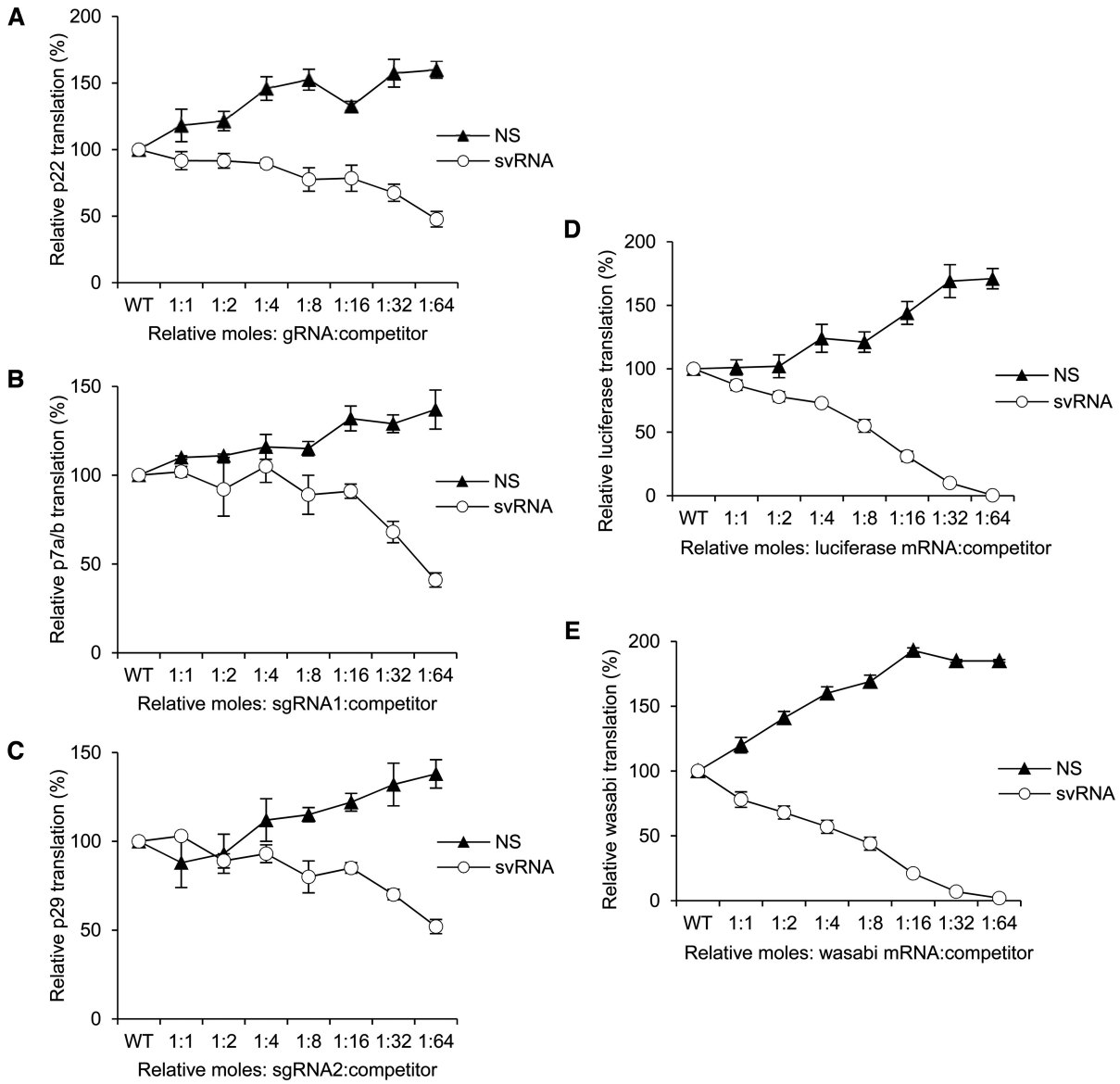

Figure 6. Translation inhibition assay using TNV-D svRNA as a competitor. (**A**) *In vitro* translation with TNV-D genomic RNA. Uncapped *in vitro* transcribed wt TNV-D genomic RNA was incubated in wheat germ extract with increasing molar amounts of 50-svRNA or a non-specific (NS) RNA in the presence of ^{35}S-labelled methionine. Levels of labeled protein were quantified and plotted for the different ratios tested. (**B**) Competition assay with sg mRNA1. (**C**) Competition assay with sg mRNA2. (**D** and **E**) Competition assay with capped luciferase and wasabi mRNAs. Results are from three independent experiments, ±SE.

In contrast, symptoms were markedly attenuated in sr10-infected leaves, which exhibited patches of small pale lesions. The yield of viral RNAs from sr10-infected plants was ∼12% that of the wt infections and, unlike for wt infections, svRNAs were not detectable and the infection did not move systemically within plants.

DISCUSSION

We have characterized an svRNA species that is generated during TNV-D infections. The svRNAs produced using recombinant Xrn1 *in vitro* were comparable in length to those generated in infected plant cells, implicating the cytosolic plant 5′-to-3′exonuclease, Xrn4, as the enzyme generating svRNAs *in vivo*. The fact that the svRNAs were generated with purified Xrn1 also indicates that other host proteins are not necessary for their production, although the possible involvement of such factors cannot be precluded. Different regions within the major svRNA species were found to be necessary for its production and distinct structural features within were determined to be essential for Xrn stalling. The implications of these and other findings are discussed.

svRNA production from a sg mRNA

Our results indicate that the majority of svRNA produced during viral infections is generated from sg mRNA1 (Figure 2D). This RNA is the more abundant of the two sg mR-

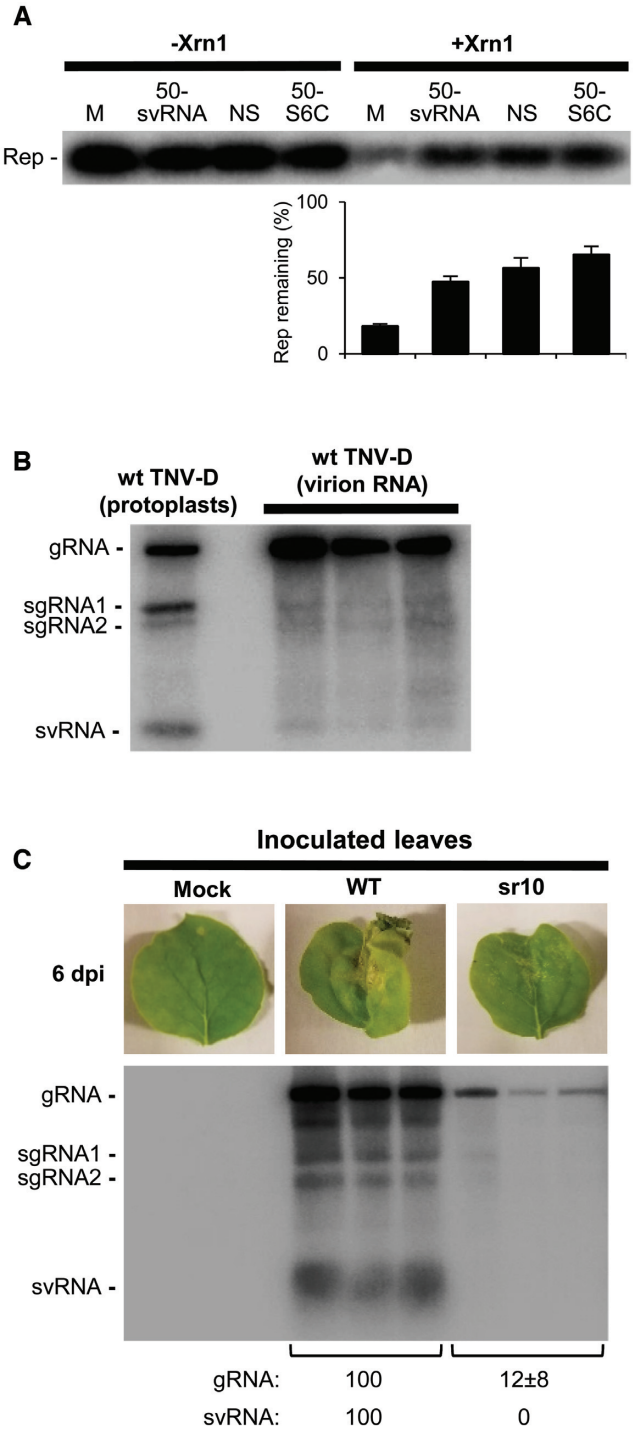

Figure 7. Functional analyses of TNV-D svRNA. (**A**) Xrn inhibition assay. A reporter RNA (Rep) was incubated with Xrn1 in the presence of competitors 50-svRNA, 50-S6C, or nonspecific RNA (NS). The amount of remaining Rep RNA was quantified by northern blotting. Results are from three independent experiments, ±SE. (**B**) Viral RNA analysis of TNV-D virions. Viral RNA was extracted from virions and analyzed by northern blotting. RNAs extracted from TNV-infected protoplasts were separated in the same gel for size comparison. Results from three independent virus isolations are shown. (**C**) Infection of *N. benthamiana* plants with svRNA-deficient mutant sr10. Total RNA was extracted from inoculated leaves of TNV-infected plants six days post infection (dpi), and analyzed by northern blotting. Representative example from three independent experiments done in triplicate.

NAs transcribed from the TNV-D genome, thus its comparatively higher level likely contributes proportionally to the production of the svRNA (Figure 1A, B). In contrast, although the viral genome accumulates to the greatest relative level in infections, it contributes minimally to svRNA production. This may be due to its efficient packaging, which could provide protection from RNases (Figure 7B). Conversely, neither sg mRNA1 nor 2 is packaged efficiently.

Both RCNMV and BNYVV produce svRNAs from genomes that also transcribe a standard sg mRNA (28,29), however the possible contribution of their sg mRNAs to the production of the svRNAs has not yet been investigated. In BYDV, inactivating sg RNA2 production in infections reduces accumulation of the svRNA, termed sgRNA3 (48), however it is not known if sgRNA3 is actually generated by Xrn (22). The possible origin of an svRNA from a transcribed viral sgRNA has been proposed for the flavivirus Japanese encephalitis virus (JEV) (49). It is well documented that many flaviviruses produce svRNAs, but these viruses do not normally transcribe sg mRNAs (11). JEV infections were shown to generate sfRNAs more efficiently in Xrn1-knockdown cells, suggesting an alternative mode for their generation. This observation, combined with *in vitro* RNA-dependent RNA polymerase promoter activity from a sequence near the stall site, prompted the notion that in JEV, sgRNA transcription mediates the production of its sfRNA (49). Further studies will be required to validate this atypical transcription-based model for svRNA production in flaviviruses.

svRNA structure

The RNA structure inhibiting Xrn exoribonucleases in TNV-D is distinct from other reported structures in terms of its (i) modularity, (ii) size, and (iii) contiguity. Other Xrn1-blocking structures have been found to be functionally modular (14,29), which contrasts our results with TNV-D, where adding sequence to the 3′-end of the structure, which alters its 3′-proximal context, abolished stalling (Figure 3). This 3′ addition would interfere with formation of the SLII/3′-terminal sequence interaction involved in genome replication. This notion is further supported by the two and three nucleotide deletions of 3′-terminal viral sequence (mutants –2 and –3) and the SLII bulge deletion (ΔSL2b) that would inhibit this interaction, and all of which yielded low levels of svRNA (Figure 3A–C). Consequently, these data implicate formation of the SLII/3′-terminal sequence interaction as an important tertiary-level stalling determinant. Residues immediately 5′-proximal to the termination site also influenced stalling function, but had more modest effects (mutants, sr1 to sr3) (Figure 3C). The substitutions in this region could potentially alter formation or stability of the downstream blocking structure. Approximately 5–6 nucleotides are predicted to reside in a protein channel leading to the active site of Xrn1 (17). In RCNMV, a sequence just downstream of the stall site is proposed to be involved in the folding of the structure mediating stalling (30). Specifically, the unwinding of a base-paired P1 stem immediately downstream of the Xrn1 stop site by Xrn1 mediates a transition of the structure from an inactive SL to an active pseudoknotted conformation; a process

termed codegradational remodelling (30). Although alternative structures are not predicted for the TNV-D region, the involvement of possible rearrangements cannot be discounted. Regardless of the mechanism of Xrn interference, the results suggest that the 5′-context of the blocking structure does influence processivity, albeit far less than the 3′-context.

The lack of modularity of the blocking RNA structure in TNV-D may in part relate to its size. Comparable functional RNA elements reported to date have been substantially smaller. For example, the linear lengths for the minimal active structures for flaviviruses, RCNMV, and BNYVV, are 72–79 nt, 43 nt and 43 nt, respectively (14,29,30). These sizes are approximately 3- to 5-fold smaller than the linear length of TNV-D sequence harbouring its stalling structure, *i.e.* 212 nt. The atomic structure of the BNYVV RNA element is yet to be explored, however those for two flaviviruses and RCNMV have been solved (15,16). Though distinct in terms of detailed conformations, all contain pseudoknots that form ring-like folds around the 5′-ends of the RNA structures. This unique type of ring structure is predicted to contact the surface of Xrn1 and act as a brace, causing it to pause. The compact nature of these RNA elements is in contrast to the region encompassing the TNV-D stall structure and may suggest that a different type of structural complexity is utilized by TNV-D to block Xrn.

Although the linear sequence involved is large, certain regions appear to be more important than others. The ability to delete the upper portion of the 3′-CITE yet maintain ∼57% activity (mutant ΔTop), rules out a critical role for this region (Figure 4A), and suggests a non-linear, or non-contiguous, arrangement of essential components. Three distinct regions were determined to be most critical; i.e. their modification led to decreases in activity to ∼10–15%. These include the lower region of the 3′-CITE (Figures 3C, 4A), SLII (Figure 3C, 4A), and the 3′-terminus (Figures 3A-C). It follows that structural coordination and/or communication between these elements is required for effective stalling. As alluded to earlier, base pairing of the SLII bulge with the 3′-terminal nucleotides is essential for TNV-D genome replication (37), and this interaction also appears to be important for formation of an effective stalling RNA structure. The requirement for specific sequence in the terminal loop of SLII and corresponding altered chemical reactivity of the lower region of the 3′-CITE upon its modification, along with reciprocal correlative evidence (Figure 4A, B), suggest an interaction between these two regions. Additionally, the hierarchical importance of sequence identity over base pairing in the lower region of the 3′-CITE (Figure 3C, and Figure 4A), suggests that non-canonical interactions and/or structural rearrangements may be involved. The detailed structural relationship between the three key structural components forming tertiary contacts, as well as the precise conformational strategy utilized to stall Xrn, remain to be elucidated.

Possible svRNA functions

Xrn-generated RNAs represent an emerging area in plant virology with a small but growing list of examples. Consequently, the functions of these RNAs in plant infections remain largely unknown (22). One exception is the svRNA of BNYVV, which has been demonstrated convincingly to be required for long-distance movement of the viral infection in plants (27,28). One can imagine a variety of possible roles for svRNAs in viral processes related to, for instance, translation, RNA replication, and/or packaging. The TNV-D svRNA inhibited translation of both viral and capped reporter mRNA *in trans* in wheat germ extract. The corresponding levels of inhibition observed in the dose-response curves for the three different viral RNA messages were similar (Figure 6A–C), suggesting that all species are supressed to comparable degrees. In contrast, the svRNA more efficiently competed against capped reporter mRNAs (Figure 6D), suggesting a possible role in preferentially downregulating cellular mRNA levels during infections. The svRNA of RCNMV was also found to inhibit translation of both viral reporter mRNAs and capped messages (29). Also, for the polymerase-generated svRNA of BYDV (24), translation of the viral genome was inhibited to a greater extent than sg mRNA1 (50). This latter observation led to the proposal that this svRNA may act as a switch to favor translation of late genes during infections. A similar regulatory role in virus translation is not predicted for TNV-D, because all viral RNAs were supressed to similar levels.

Other possible functions for the TNV-D svRNA could be to supress Xrn4 activity during infections or facilitate packaging. For TNV-D, our *in vitro* results did not support a role for its svRNA in inhibiting Xrn activity (Figure 7A), which contrasts results from other Xrn1 blocking structures in mammalian viruses (18,19,51). One could imagine that supressing Xrn4 activity during infections could be beneficial to the survival of uncapped viral RNA genomes like TNV-D. The observed lack of inhibitory activity on the enzyme could be related to the modest level of stalling (∼4.3%), which probably would not notably affect enzyme turnover. As for packaging, a small but readily detectable amount of svRNA was present in virions (Figure 7B). The svRNA of RCNMV is also packaged into virions, and could mediate assembly and/or promote particle stability (29). However, the TNV-D svRNA, and the two sg mRNAs, are not packaged efficiently. Consequently, the incorporation of these 3′-terminal sg mRNAs and svRNA in virions may be inadvertent.

Demonstrating a function for svRNA in plants has been particularly challenging. Aside from BNYVV (28,29), *in vivo* studies of viral genomes, where svRNA production has been inactivated, have resulted in only minor effects (24,29,38). Our testing of an svRNA-deficient TNV-D mutant in plants showed major differences in symptomology, viral RNA accumulation, and movement (Figure 7C). Nonetheless, it cannot be precluded that additional viral processes were affected by the modifications, even though second-site structural perturbations were not observed (Figure 4B). Indeed, the structural features that make the svRNA resistant to Xrn overlap with, or are highly integrated with, the structural elements important for a variety of viral processes. Moreover, new functions for components in this region are being discovered; *i.e.* the wt loop sequence of SLII is also required for efficient translational readthrough (37). It is thus possible that the SLII loop/lower 3′-CITE interaction needed for Xrn stalling

is also required for readthrough activity. Further detailed analyses of these overlapping features will be required to design mutants that are exclusively deficient in svRNA production.

In addition to TNV-D (Betanecrovirus) and RCNMV (Dianthovirus), at least three other genera in family Tombusviridae generate 3′-terminal svRNAs that likely originate from Xrn4 digestion. These include, tombusviruses (32), machlomoviruses (34) and carmoviruses (52). Other genera in this family may also generate svRNAs, however they may have either been overlooked or dismissed as nonrelevant degradation products (22). Recently, a bioinformatics approach was used to identify additional functional RCNMV-like stalling structures in umbraviruses (family Tombusviridae), as well as polero- and enamoviruses (family Luteoviridae) (53). Moreover, some of the svRNAs identified were predicted to encode proteins, suggesting that they could function as mRNAs for viral protein production. Their prevalence in multiple virus groups and elusive functions make Xrn-resistant RNAs intriguing subjects for further investigation.

SUPPLEMENTARY DATA

Supplementary Data are available at NAR Online.

ACKNOWLEDGEMENTS

We thank Robert Coutts for the TNV-D clone and members of our laboratory for reviewing the manuscript.

FUNDING

Natural Sciences and Engineering Research Council of Canada (NSERC); Ontario Graduate Scholarship (to C.D.G.); NSERC graduate fellowship (to L.R.N.). Funding for open access charge: York University Open Access Author Fund.
Conflict of interest statement. None declared.

REFERENCES

1. Molleston,J.M. and Cherry,S. (2017) Attacked from all Sides: RNA decay in antiviral defense. *Viruses*, **9**, E2.
2. Stevens,A. (2001) 5′-exoribonuclease 1: Xrn1. *Methods Enzymol.*, **342**, 251–259.
3. Jones,C.I., Zabolotskaya,M.V. and Newbury,S.F. (2012) The 5′ → 3′ exoribonuclease XRN1/Pacman and its functions in cellular processes and development. *Wiley Interdiscip. Rev. RNA*, **3**, 455–468.
4. Łabno,A., Tomecki,R. and Dziembowski,A. (2016) Cytoplasmic RNA decay pathways—enzymes and mechanisms. *Biochim. Biophys. Acta.*, **1863**, 3125–3147.
5. Poole,T.L. and Stevens,A. (1997) Structural modifications of RNA influence the 5′ exoribonucleolytic hydrolysis by XRN1 and HKE1 of Saccharomyces cerevisiae. *Biochem. Biophys. Res. Commun.*, **235**, 799–805.
6. Jaag,H.M. and Nagy,P.D. (2009) Silencing of Nicotiana benthamiana Xrn4p exoribonuclease promotes tombusvirus RNA accumulation and recombination. *Virology*, **386**, 344–352.
7. Li,Y., Yamane,D. and Lemon,S.M. (2015) Dissecting the roles of the 5′ exoribonucleases Xrn1 and Xrn2 in restricting hepatitis C virus replication. *J. Virol.*, **89**, 4857–4865.
8. Lee,C.C., Lin,T.L., Lin,J.W., Han,Y.T., Huang,Y.T., Hsu,Y.H. and Meng,M. (2016) Promotion of bamboo mosaic virus accumulation in Nicotiana benthamiana by 5′→3′ exonuclease NbXRN4. *Front. Microbiol.*, **6**, 1508.
9. Clarke,B.D., Roby,J.A., Slonchak,A. and Khromykh,A.A. (2015) Functional non-coding RNAs derived from the flavivirus 3′ untranslated region. *Virus Res.*, **206**, 53–61.
10. Pijlman,G.P., Funk,A., Kondratieva,N., Leung,J., Torres,S., van der Aa,L., Liu,W.J., Palmenberg,A.C., Shi,P.Y., Hall,R.A. *et al.* (2008) A highly structured, nuclease-resistant, noncoding RNA produced by flaviviruses is required for pathogenicity. *Cell Host Microbe*, **4**, 579–591.
11. Slonchak,A. and Khromykh,A.A. (2018) Subgenomic flaviviral RNAs: what do we know after the first decade of research. *Antiviral Res.*, **159**, 13–25.
12. Funk,A., Truong,K., Nagasaki,T., Torres,S., Floden,N., Balmori Melian,E., Edmonds,J., Dong,H., Shi,P.Y. and Khromykh,A.A. (2010) RNA structures required for production of subgenomic flavivirus RNA. *J. Virol.*, **84**, 11407–11417.
13 Silva,P.A., Pereira,C.F., Dalebout,T.J., Spaan,W.J. and Bredenbeek,P.J. (2010) An RNA pseudoknot is required for production of yellow fever virus subgenomic RNA by the host nuclease XRN1. *J. Virol.*, **84**, 11395–113406.
14. Chapman,E.G., Moon,S.L., Wilusz,J. and Kieft,J.S. (2014) RNA structures that resist degradation by Xrn1 produce a pathogenic Dengue virus RNA. *Elife*, **3**, e01892.
15. Chapman,E.G., Costantino,D.A., Rabe,J.L., Moon,S.L., Wilusz,J., Nix,J.C. and Kieft,J.S. (2014). The structural basis of pathogenic subgenomic flavivirus RNA (sfRNA) production. *Science*, **344**, 307–310.
16. Akiyama,B.M., Laurence,H.M., Massey,A.R., Costantino,D.A., Xie,X., Yang,Y., Shi,P.Y., Nix,J.C., Beckham,J.D. and Kieft,J.S. (2016) Zika virus produces noncoding RNAs using a multi-pseudoknot structure that confounds a cellular exonuclease. *Science*, **354**, 1148–1152.
17. MacFadden,A., O'Donoghue,Z., Silva,P.A.G.C., Chapman,E.G., Olsthoorn,R.C., Sterken,M.G., Pijlman,G.P., Bredenbeek,P.J. and Kieft,J.S. (2018) Mechanism and structural diversity of exoribonuclease-resistant RNA structures in flaviviral RNAs. *Nat. Commun.*, **9**, 119.
18. Moon,S.L., Blackinton,J.G., Anderson,J.R., Dozier,M.K., Dodd,B.J., Keene,J.D., Wilusz,C.J., Bradrick,S.S. and Wilusz,J. (2015) XRN1 stalling in the 5′ UTR of hepatitis C virus and bovine viral diarrhea virus is associated with dysregulated host mRNA stability. *PLoS Pathog.*, **11**, e1004708.
19. Charley,P.A., Wilusz,C.J. and Wilusz,J. (2018) Identification of phlebovirus and arenavirus RNA sequences that stall and repress the exoribonuclease XRN1. *J. Biol. Chem.*, **293**, 285–295.
20. Nagarajan,V.K., Jones,C.I., Newbury,S.F. and Green,P.J. (2013) XRN 5′→3′ exoribonucleases: structure, mechanisms and functions. *Biochim. Biophys. Acta.*, **1829**, 590–603.
21. Peng,J., Yang,J., Yan,F., Lu,Y., Jiang,S., Lin,L., Zheng,H., Chen,H. and Chen,J. (2011) Silencing of NbXrn4 facilitates the systemic infection of Tobacco mosaic virus in Nicotiana benthamiana. *Virus Res.*, **158**, 268–270.
22. Miller,W.A., Shen,R., Staplin,W. and Kanodia,P. (2016) Noncoding RNAs of plant viruses and viroids: sponges of host translation and rna interference machinery. *Mol. Plant Microbe Interact.*, **29**, 156–164.
23. Kelly,L., Gerlach,W.L. and Waterhouse,P.M. (1994) Characterisation of the subgenomic RNAs of an Australian isolate of barley yellow dwarf luteovirus. *Virology*, **202**, 565–573.
24. Koev,G. and Miller,W.A. (2000) A positive-strand RNA virus with three very different subgenomic RNA promoters. *J. Virol.*, **74**, 5988–5996.
25. Yamagishi,N., Terauchi,H., Kanematsu,S. and Hidaka,S. (2003) Characterization of the small subgenomic RNA of soybean dwarf virus. *Arch. Virol.*, **148**, 1827–1834.
26. Peltier,C., Klein,E., Hleibieh,K., D'Alonzo,M., Hammann,P., Bouzoubaa,S., Ratti,C. and Gilmer,D. (2012) Beet necrotic yellow vein virus subgenomic RNA3 is a cleavage product leading to stable non-coding RNA required for long-distance movement. *J. Gen. Virol.*, **93**, 1093–1102.
27. Flobinus,A., Chevigny,N., Charley,P.A., Seissler,T., Klein,E., Bleykasten-Grosshans,C., Ratti,C., Bouzoubaa,S., Wilusz,J. and Gilmer,D. (2018) Beet Necrotic yellow vein virus noncoding RNA production depends on a 5′→3′ Xrn exoribonuclease activity. *Viruses*, **10**, E137.

28. Dilweg,I.W., Gultyaev,A.P. and Olsthoorn,R.C. (2019) Structural features of an Xrn1-resistant plant virus RNA. *RNA Biol.*, **16**, 838–845.
29. Iwakawa,H.O., Mizumoto,H., Nagano,H., Imoto,Y., Takigawa,K., Sarawaneeyaruk,S., Kaido,M., Mise,K. and Okuno,T. (2008) A viral noncoding RNA generated by cis-element-mediated protection against 5′→3′ RNA decay represses both cap-independent and cap-dependent translation. *J. Virol.*, **82**, 10162–10174.
30. Steckelberg,A.L., Akiyama,B.M., Costantino,D.A., Sit,T.L., Nix,J.C. and Kieft,J.S. (2018) A folded viral noncoding RNA blocks host cell exoribonucleases through a conformationally dynamic RNA structure. *Proc. Natl. Acad. Sci. U.S.A.*, **115**, 6404–6409
31. Miller,W.A., Shen,R., Staplin,W. and Kanodia,P. (2016) Noncoding RNAs of plant viruses and viroids: sponges of host translation and RNA interference machinery. *Mol. Plant Microbe Interact.*, **29**, 156–164.
32. Jiwan,S.D., Wu,B. and White,K.A. (2011) Subgenomic mRNA transcription in Tobacco necrosis virus. *Virology*, **418**, 1–11.
32. Johnston,J.C. and Rochon,D.M. (1995) Deletion analysis of the promoter for the cucumber necrosis virus 0.9-kb subgenomic RNA. *Virology*, **214**, 100–109.
34. Scheets,K. (2000) Maize chlorotic mottle machlomovirus expresses its coat protein from a 1.47-kb subgenomic RNA and makes a 0.34-kb subgenomic RNA. *Virology*, **267**, 90–101.
35. Coutts,R.H., Rigden,J.E., Slabas,A.R., Lomonossoff,G.P. and Wise,P.J. (1991) The complete nucleotide sequence of Tobacco necrosis virus strain D. *J. Gen. Virol.*, **72**, 1521–1529.
36. Newburn,L.R., Nicholson,B.L., Yosefi,M., Cimino,P.A. and White,K.A. (2014) Translational readthrough in Tobacco necrosis virus-D. *Virology*, **450-451**, 258–265.
37. Newburn,L.R. and White,K.A. (2017) Atypical RNA elements modulate translational readthrough in Tobacco necrosis virus D. *J. Virol.*, **91**, e02443-16.
38. Shen,R. and Miller,W.A. (2004) The 3′ untranslated region of Tobacco necrosis virus RNA contains a barley yellow dwarf virus-like cap-independent translation element. *J. Virol.*, **78**, 4655–4664.
39. Kraft,J.J., Treder,K., Peterson,M.S. and Miller,W.A. (2013) Cation-dependent folding of 3′ cap-independent translation elements facilitates interaction of a 17-nucleotide conserved sequence with eIF4G. *Nucleic Acids Res.*, **41**, 3398–3413.
40. Chkuaseli,T., Newburn,L.R., Bakhshinyan,D. and White,K.A. (2015) Protein expression strategies in Tobacco necrosis virus-D. *Virology*, **486**, 54–62.
41. Gunawardene,C.D., Jaluba,K. and White,K.A. (2015) Conserved motifs in a tombusvirus polymerase modulate genome replication, subgenomic transcription, and amplification of defective interfering RNAs. *J. Virol.*, **89**, 3236–3246.
42. White,K.A. and Morris,T.J. (1994) Nonhomologous RNA recombination in tombusviruses: generation and evolution of defective interfering RNAs by stepwise deletions. *J. Virol.*, **68**, 14–24.
43. Regulski,E.E. and Breaker,R.R. (2008) In-line probing analysis of riboswitches. *Methods Mol. Biol.*, **419**, 53–67.
44. Nicholson,B.L., Zaslaver,O., Mayberry,L.K., Browning,K.S. and White,K.A. (2013) Tombusvirus Y-shaped translational enhancer forms a complex with eIF4F and can be functionally replaced by heterologous translational enhancers. *J. Virol.*, **87**, 1872–1883.
45. Hillman,B.I., Morris,T.J. and Schlegel,D.E. (1985) Effects of low molecular- weight RNA and temperature on tomato bushy stunt virus symptom expression. *Phytopathology*, **75**, 361–365.
46. Wang,Z., Kraft,J.J., Hui,A.Y. and Miller,W.A. (2010) Structural plasticity of Barley yellow dwarf virus-like cap-independent translation elements in four genera of plant viral RNAs. *Virology*, **402**, 177–186.
47. Molinaro,M. and Tinoco,I. Jr (1995) Use of ultra stable UNCG tetraloop hairpins to fold RNA structures: thermodynamic and spectroscopic applications. *Nucleic Acids Res.*, **23**, 3056–3063.
48. Shen,R., Rakotondrafara,A.M. and Miller,W.A. (2006) Trans regulation of cap-independent translation by a viral subgenomic RNA. *J. Virol.*, **80**, 10045–10054.
49. Chen,Y.S., Fan,Y.H., Tien,C.F., Yueh,A. and Chang,R.Y. (2018) The conserved stem-loop II structure at the 3′ untranslated region of Japanese encephalitis virus genome is required for the formation of subgenomic flaviviral RNA. *PLoS One*, **13**, e0201250.
50. Wang,S., Guo,L., Allen,E. and Miller,W.A. (1999) A potential mechanism for selective control of cap-independent translation by a viral RNA sequence in cis and in trans. *RNA*, **5**, 728–738.
51. Moon,S.L., Anderson,J.R., Kumagai,Y., Wilusz,C.J., Akira,S., Khromykh,A.A. and Wilusz,J. (2012) A noncoding RNA produced by arthropod-borne flaviviruses inhibits the cellular exoribonuclease XRN1 and alters host mRNA stability. *RNA*, **18**, 2029–2040.
52. Zhang,S., Sun,R., Guo,Q., Zhang,X.F. and Qu,F. (2018) Repression of turnip crinkle virus replication by its replication protein p88. *Virology*, **526**, 165–172.
53. Steckelberg,A., Vicens,Q. and Kieft,J.S. Pervasiveness of exoribonuclease-resistant RNAs in plant viruses suggests new roles for these conserved RNA structures. *mBio.*, **9**, e02461-18.